Unraveling mechanisms of vascular remodeling in arteriovenous fistulas for hemodialysis

Wong, C.Y.

Chapter 3

Vascular remodeling and intimal hyperplasia in a novel murine model of arteriovenous fistula failure

C.Y. Wong, M.R. de Vries, Y. Wang, J.R. van der Vorst, A.L. Vahrmeijer , A.J. van Zonneveld, P. Roy-Chaudhury, T.J. Rabelink, P.H.A Quax and J.I. Rotmans

J Vasc Surg. 2014 Jan;59(1):192-201

Abstract

Objective

The arteriovenous fistula (AVF) still suffers from a high number of failures caused by insufficient outward remodeling and intimal hyperplasia (IH) formation from which the exact mechanism is largely unknown. A suitable animal model is of vital importance in the unraveling of the underlying pathophysiology. However, current murine models of AVF failure do not incorporate the surgical configuration that is commonly used in humans. Since the hemodynamic profile is one of the key determinants that play a role in vascular remodeling in the AVF, it is preferable to use this same configuration in an animal model. Here we describe a novel murine model of arteriovenous fistula failure, in which the configuration (end-to-side) is similar to what is most frequently performed in humans.

Methods

An AVF was created in 45 C57BL/6 mice by anastomosing the end of a branch of the external jugular vein to the side of the common carotid artery with interrupted sutures. The fistulas were harvested and analyzed histologically at days 7, 14 and 28. Identical veins of unoperated mice served as controls. Intravenous near-infrared fluorescencent fluorophores were used to assess the patency of the fistula.

Results

The patency rates at days 7, 14 and 28 days were 88%, 90% and 50%, respectively. The mean circumference increased up to day 14 with a maximum 1.4-fold increase at day 7 as compared to the control group (1.82±0.7mm vs 1.33±0.3mm;P= .443). Between days 14 and 28, the circumference remained constant (2.36±0.2mm vs 2.45±0.2mm;P= .996). At 7 days after surgery, the intimal area consisted mainly of an acellular layer that was structurally analogous to a focal adherent thrombus Starting at 14 days after surgery, venous IH increased significantly as compared to the unoperated group (14 days:115090±22594μm^2, 28 days:234619±47828μm^2, unoperated group:2368±1056μm^2;P= .001 and P< .001, respectively) and was mainly composed of α-smooth muscle actin-positive cells. We observed leukocytes in the adventitial side of the vein at all time points.

Conclusion

Our novel murine arteriovenous fistula model, which incorporates a clinically relevant configuration of the anastomosis, displays similar features that are characteristic of failing human fistulas. Moreover, our findings suggest that both coagulation and inflammation could potentially play an important role in the formation of intimal hyperplasia and subsequent arteriovenous fistula failure. Near infrared fluoroscopy proved to be a suitable alternative for conventional imaging techniques. We conclude that this murine AVF-model is a valuable addition to the AVF animal model arsenal.

Clinical relevance

The autologous arteriovenous fistula is considered to be the preferred choice of vascular access in hemodialysis. However, this type of vascular access suffers from a high failure rate of which the exact pathophysiology is poorly understood. The use of a clinically relevant murine model provides us with a tool to unravel the pathophysiology and also to develop new therapeutic strategies that can improve the patency of the arteriovenous fistula in hemodialysis patients.

Introduction

A durable vascular access is of vital importance for patients on chronic hemodialysis. In view of their superior patency rates, the construction of native arteriovenous fistulas (AVF) is currently the preferred choice for vascular access. However, the utility of AVFs is hampered by two distinct causes of failure: (1) an initial failure to mature; and (2) the later development of stenotic lesions in the venous outflow tract. The exact pathophysiology that results in maturation failure is unclear although both intimal hyperplasia (IH) and impaired outward remodelling (OR) seem to contribute [1]. Various studies report poor one-year primary patency rates of AVFs not exceeding 60-65% [2-4].

To date, numerous animal models [5-17] have been designed to study AVF failure. While large animals such as pigs are more suitable for intervention studies, murine models have the greatest potential to gain more insight in the molecular mechanisms underlying this pathologic process due to the availability of transgenic mice.

In previous studies, two groups have described a murine AVF model in which the fistula was constructed in an end-to-end manner [7, 17]. In 2006, an improved model was introduced by Castier et al. [5, 18] where the end of the common carotid artery is connected to the side of the external jugular vein. However, in hemodialysis patients, AVFs are usually constructed by anastomosing the end of a vein to the side of an artery. The exact configuration of the AVF is crucial since it determines the hemodynamic profile [19], an important contributor to endothelial dysfunction and subsequent development of IH [20-22]. Therefore, incorporating an AVF configuration resembling the human situation is preferable. In the present study, we developed a novel murine model with an identical anatomical configuration as utilized in humans. In our analysis, we focused on outward remodeling as well as the formation of IH in the venous outflow tract.

Material and Methods

Animals and study design

The Institutional Committee for Animal Welfare at the LUMC approved all experiments. Forty-five male C57bl6 mice (Charles River) aged 8-13 weeks were used. Unilateral AVFs were created in an end-to-side manner between the dorsomedial branch of the external jugular vein and the common carotid artery. The animals were sacrificed at days 7, 14 and 28 after the surgical procedure. Identical veins of unoperated mice served as controls.

Anesthesia, analgesia and anticoagulant therapy

At the start of the procedure, animals were injected subcutaneously with buprenorphin (0.1 mg/kg) (MSD, Whitehouse Station, NJ, USA) and 0.5 mL saline. Isoflurane inhalation anesthesia with oxygen (40%) enriched air was used, with isoflurane concentrations of 4% for induction and 1.5% for maintenance. To prevent acute AVF thrombosis, acetylsalicylic acid (Sigma, St Louis, MO, USA) dosed at 30 mg/kg was dissolved in drinking water. However, this approach was not successful as it caused severe hemorrhage at the anastomosis. As an alternative, heparin was administered intravenously at a dose of 0.2 IU/gram bodyweight (LEO Pharma, Ballerup, Denmark).

Surgical procedure

After anesthetizing the animal, eyes were covered with an ointment (Oculentum simplex, Pharmachemie BV, Haarlem, The Netherlands) and the surgical area was shaved. Next, the animal was fixed in a supine position on a heating blanket. The skin was disinfected and a ventral midline incision was made in the neck under a dissecting microscope (M80, Leica, Wetzlar, Germany). After dissecting the dorsomedial distal branch of the right external jugular vein, a vascular clamp (S&T, Neuhausen, Switzerland) was placed proximally and a 10.0 ligature (BBraun, Melsungen, Germany) was placed distally followed by transection of the vein just proximal from the ligature. (Fig 1, A-E) The vein was then rinsed with saline containing 100 IU/mL heparin. The right sternocleidomastoid muscle was then dissected and ligated proximally and distally with a 6.0 suture thread (BBraun, Melsungen, Germany). The muscle was then transsected between the two ligations with a heat cauterizer (Fine Science Tools, Heidelberg, Germany). Next, the right common carotid artery was dissected and clamped, followed by an incision of approximately 1.0 mm longitudinally with micro-scissors (Fine Science Tools, Heidelberg, Germany). Subsequently, the carotid artery was rinsed with heparin (100 IU/mL), whereupon the end of the vein was anastomized to the side of the artery using 10.0 interrupted sutures (BBraun, Melsungen, Germany). Heparin (0.2 IU/gram bodyweight) was injected intravenously halfway during suturing. After completion of the anastomosis, the remaining clamps were removed and patency was assessed. The skin was closed with a 6.0 running suture suture (BBraun, Melsungen, Germany). A more detailed description is available in the online supplement.

Following completion of the surgery 0.5 mL of saline was injected subcutaneously and the animals were kept warm until full recovery. A peroperative patent AVF, followed by a complete recovery from the anesthesia, was considered a surgical success.

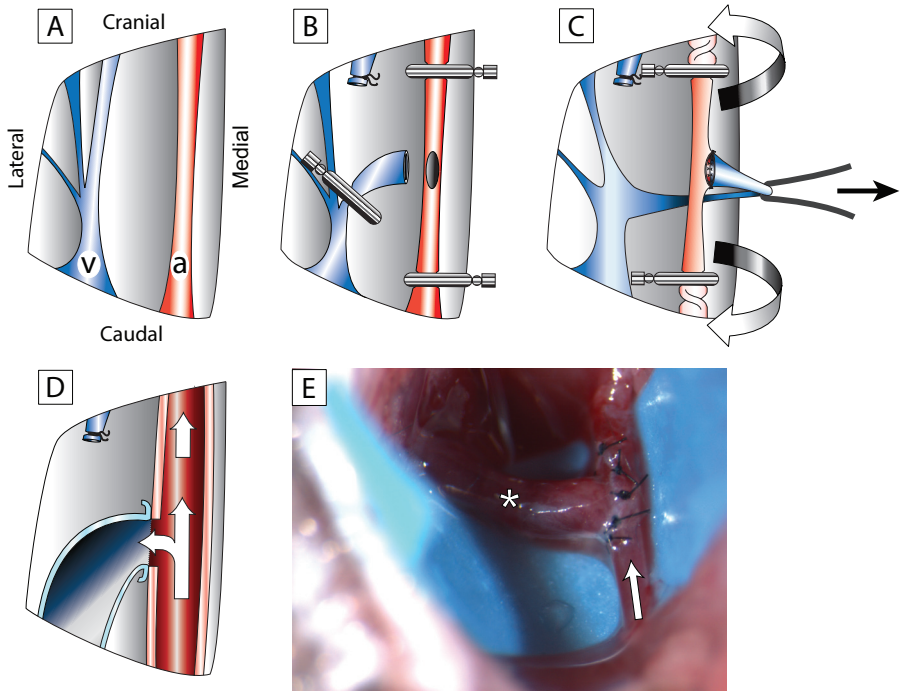

Figure 1. Surgical procedure. A, Dissection of the carotid artery (*a*) and external jugular vein (*v*). B, After placement of vascular clamps and ligation of the vein, an incision was made in the artery, followed by the transection of the vein. C, After the front side of the anastomosis is completed with interrupted sutures, the backside is exposed using a suture wire and by simultaneously twisting the vascular clamps 180°. D, Blood flow direction (*arrows*) in the arteriovenous fistula (AVF). E, Photograph of completed AVF. The *white arrow* depicts blood flow in the artery, and the *asterisk* (*) designates the venous outflow tract.

Near-infrared fluorescence imaging

To assess direct postoperative AVF patency and at the time of sacrifice (day 14 or day 28), near infrared fluorescence (NIRF) imaging was used as previously described [23 24]. Each animal received 200 µL via the femoral vein of a 500 µM indocyanine green solution (ICG) (Pulsion Medical Systems, Munich, Germany) that was dissolved in a 20% human serum albumin (HSA) (Sanquin, Amsterdam,The Netherlands).

Directly after the injection, the Fluorescence Assisted Resection and Exploration (FLARE) imaging system (Center for Molecular Imaging, Boston, MA, USA) was positioned approximately 46 cm above the AVF and video images were captured with 30 frames-per-second. Multiple video channels (color video, 700 nm and 800 nm) were obtained simultaneously with

60 milliseconds (16.7 Hz) exposure times. After computer-controlled image acquisition, color video and NIRF images were displayed individually and/or merged in real-time. The 800 nm channel was used for imaging ICG.

Tissue harvesting and processing

Upon sacrifice, animals received an intraperitoneal injection with an anesthetic-mixture containing midazolam (5 mg/kg) (Roche, Basel, Switzerland), medetomidine (0.5 mg/kg) (Orion, Espoo, Finland) and fentanyl (0.05 mg/kg) (Janssen, High Wycombe, UK) whereupon a reincision was made over the scar. The AVF was dissected and patency was assessed. After a thoracotomy, the inferior vena cava was transected followed by an intracardiac perfusion with subsequently 4% formalin. The tissue was processed to paraffin and sections of 5 μm were made perpendicular to the vein at 12 locations with an interval of 150 μm. The small size of the murine vasculature and the configuration of the AVF preclude simultaneous perpendicular analysis of the carotid artery and the jugular vein. Since most of the stenotic lesions in human AVFs occur in the venous outflow tract, we focused our analysis on the vein.

Morphometric analysis

A histochemical staining with hematoxylin, phloxin and saffron (HPS) was used for a morphological overview. Fibrin deposition was assessed by using a Movat pentachrome staining. Morphometric analysis was performed on Weigert's elastin stained sections. All venous sections were analyzed using quantitative imaging software (Qwin, Leica, Wetzlar, Germany). The intimal area was calculated by subtracting the luminal area from the area within the internal elastic lamina (IEL). The circumference of the vessel was determined by the length of the IEL (Fig 2, *A*). The percentage stenosis was defined as the intimal area divided by the intimal area plus the lumen area (intima/(intima+lumen) X 100). AVFs were defined patent histologically, when the maximum stenosis percentage in all included venous sections was ≤ 95%. Additionally, the venous sections were divided in 4 equal segments of 300 μm (A-D) by grouping 2 consecutive slides starting from the area closest to the anastomosis (Fig 3, *C*). Results are expressed as mean ± standard error of the mean.

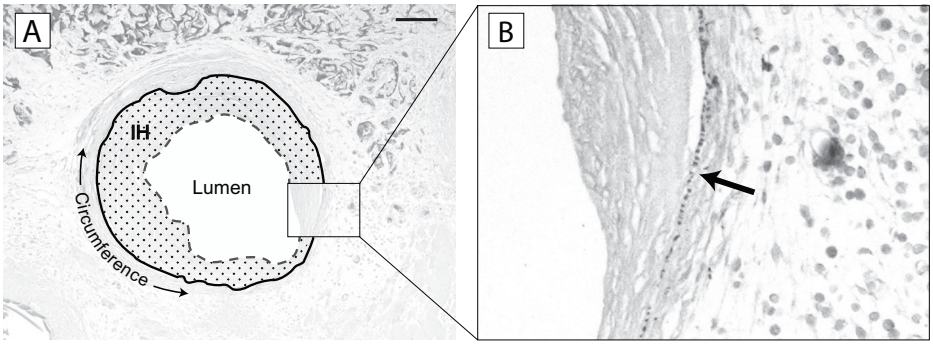

Figure 2. Morphometric parameters and fragmentation of internal elastic lamina (IEL). Venous section in the arteriovenous fistula (AVF) stained with Weigert elastin. (A), The IEL, traced in *black*, is used to quantify the circumference. Intimal hyperplasia (*IH*) and luminal (*lumen*) area are shown. (B), High magnification photomicrograph shows fragmentation of the IEL, which is indicated by the *black arrow* (original magnification, ×100; *scale bar*: 100 μm).

Collagen quantification

Collagen content was determined in sirius red stained sections using quantitative imaging software (Qwin, Leica, Wetzlar, Germany). This was measured in the whole vessel and was expressed as total positive surface area (μm2) and as positive area divided by the total vessel area (%).

Immunohistochemical analysis

Serial sections from each AVF were stained with the following antibodies: anti- α-smooth muscle actin (α-sma) for vascular smooth muscle cells (VSMC) and myofibroblasts, at 1:1000 dilution; (Dako, Glostrup, Denmark); anti-CD31 for endothelial cells, at 1:200 dilution (Abcam, Cambridge, UK); anti-CD45 for leukocytes, at 1:200 dilution (BD Pharmingen, San Diego, California, USA). Slides were digitized at a resolution of 2080 x 1542 by a camera connected to a microscope (Carl Zeiss, Oberkochen, Germany). Detailed protocols of the stainings are listed in the supplement.

Statistical analysis

Results are expressed as mean ± standard error of the mean. Comparison between the time points was performed by one-way ANOVA followed by a Tukey HSD test. Differences were considered statistically significant at a value of $P < .05$.

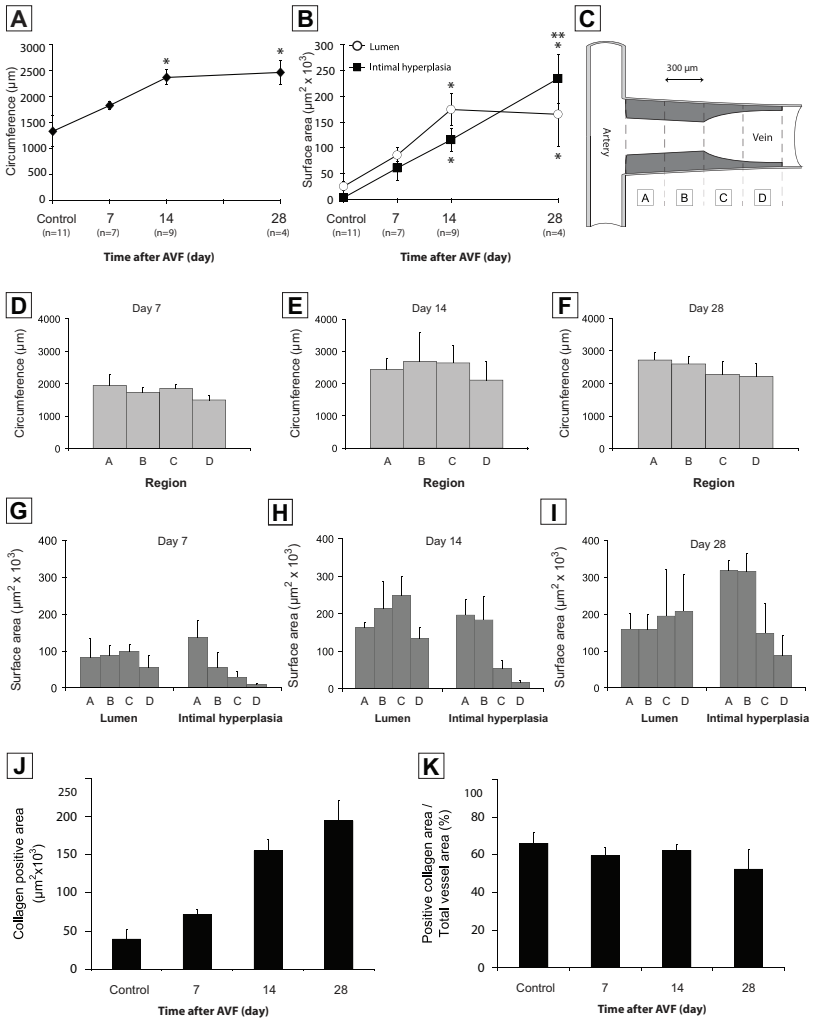

Figure 3. Quantification of outward remodeling (OR) and intimal hyperplasia (IH). (A), OR was present in the first 14 days after arteriovenous fistula (*AVF*) creation. (B), IH increased progressively in time, whereas the luminal area only increased in the first 14 days after AVF placement due to a reduction in OR after this time point. Furthermore, the increase in IH between consecutive time points was significant between days 14 and 28. (C), The venous outflow tract was divided in four equal segments of 300 µm (*A-D*) and shows that the maximum IH (*shaded area*) was located at the site closest to the anastomosis. OR at days (D) 7, (E) 14, and (F) 28 and luminal area at days (G) 7, (H) 14, and (I) 28 were not differently distributed in the vein. At days 14 and 28, IH was the highest in the first 600 µm. (J), The total amount of collagen increased in time. (K), However, the amount of collagen divided by the total vessel area remained the same between the control and arterialized vein. $^{*}P < .05$ compared with control. $^{**}P < .05$ compared with the previous time point. Mean data are presented with the standard error of the mean (*error bars*).

Results

Surgical outcome

In total, 45 mice were operated and in 30 mice the surgical procedure was successful (67%). The main cause of failure was hemorrhage (60%), followed by acute thrombosis (27%) and anesthesia related death (13%). In the group where the surgical intervention was successful, 3 mice died post-operatively of unknown causes and 1 mouse developed a wound abscess. These 4 mice were excluded from the study. The remaining 26 mice were sacrificed at days 7 (8 mice), 14 (10 mice) and 28 (8 mice) after surgery. Eleven animals without AVF surgery served as control. The average time of the surgical procedure was 60 minutes.

Patency

Patency of the AVF was assessed visually using the dissecting microscope at time of sacrifice and was confirmed histologically. This resulted in patency rates of 88%, 90% and 50% at days 7, 14 and 28, respectively. In addition, the patency was assessed in 10 mice by NIRF. As shown in Fig 4, *A-C*, representative NIRF images are depicted of a patent AVF directly after creation and at 28 days.

The patency assessed by NIRF matched the visual assessment in 10 out of 11 cases (91%). In the remaining mouse, the AVF appeared patent by NIRF while no perfusion could be observed macroscopically. A representative movie of the patency assessment using NIRF is available as online supplement.

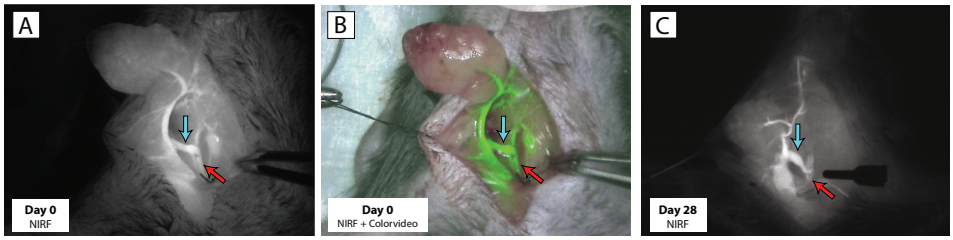

Figure 4. Visualization of the arteriovenous fistula (AVF) with near-infrared fluorescence imaging. The proximal carotid artery and venous outflow tract are depicted by a *red* and *blue arrow*, respectively. (A), Intravenous administration of indocyanine green (*white*) that is detected at 800 nm using a fluorescence-assisted resection and exploration (FLARE) imaging system indicates AVF patency directly after completion of the surgical intervention. (B), Merged image of color video and 800-nm near-infrared fluorescence channel. (C), At 28 days after surgery, the luminal area is reduced in the perianastomotic area due to intimal hyperplasia (IH).

Morphometric analysis

For the quantification of OR and IH, only patent AVFs were included in the analysis (7, 8 and 4 mice for 7, 14 and 28 days of follow-up, respectively).

Outward remodeling

The venous circumference at days 14 (2.36 ± 0.15 mm) and 28 (2.45 ± 0.24 mm) was higher compared to that of the unoperated control mice (1.33 ± 0.30 mm; P = .01 and P= .037, respectively). The highest increase in mean venous circumference (1.4-fold) was observed within 7 days after surgery (1.33 ± 0.30 mm vs 1.82 ± 0.07 mm; P = .443). Between days 7 and 14, a 1.3-fold increase was observed (P = .397), whereas no increase in venous circumference was observed from days 14 to 28 (P = .996). (Fig 3, *A*).

No difference in OR was observed between various sections of the AVF (Fig 3, *D-F*). Of note, the venous circumference of the occluded AVFs (1.69 ± 0.2 mm) at day 28 was smaller when compared to patent AVF (2.45 ± 0.2 mm) at the same time point. In all AVFs, we observed fragmentation of the IEL in the venous outflow tract (Fig 2, *B*).

Intimal hyperplasia and luminal area

Already 7 days after surgery, we observed intimal hyperplasia (60138 ± 23626 μm^2) in the venous outflow tract (Fig 5, *B-D*). This area further increased at days 14 and 28 (115090 ± 22594 μm^2 and 234619 ± 47828 μm^2, respectively) and was significantly higher as compared to control mice (2368 ± 1056 μm^2 ; P = .001 and P <.001). (Fig 3, *B*). Detailed analysis of the various sections within the venous outflow tract revealed that IH was most prominent in the first 600 μm from the anastomosis (Fig 3, *G-I*). The combined effect of the OR process and IH resulted in a markedly higher luminal area both at day 14 and 28 (173965 ± 30829 μm^2 and 164842 ± 63411 μm^2) when compared to the control (24679 ± 8462 μm^2 ; P< .001 and P= .010, respectively). Between the consecutive time points, we observed a 3.5-fold increase in the luminal area at day 7 (85693 ± 13541 μm^2) as compared to the control veins (P= .294). Between days 7 and 14, a 2-fold increase in lumen area was observed (P= .082). At day 28 the luminal area of the patent AVFs decreased with 5% compared to day 14 (P= .996) (Fig 3, *B*).

The mean stenosis at days 7, 14 and 28 were 30%, 38% and 59%, respectively. Seven days after surgery, the highest percentage of stenosis was observed in the first 300 μm from the anastomosis (segment A). At days 14 and 28 after surgery, the percentage stenosis was the highest in segment A and B (data not shown). In the occluded AVFs at day 28, IH was 23% lower compared to patent vessels at the same time point (180866 ± 49332 μm2 vs 234619 ± 47828 μm^2).

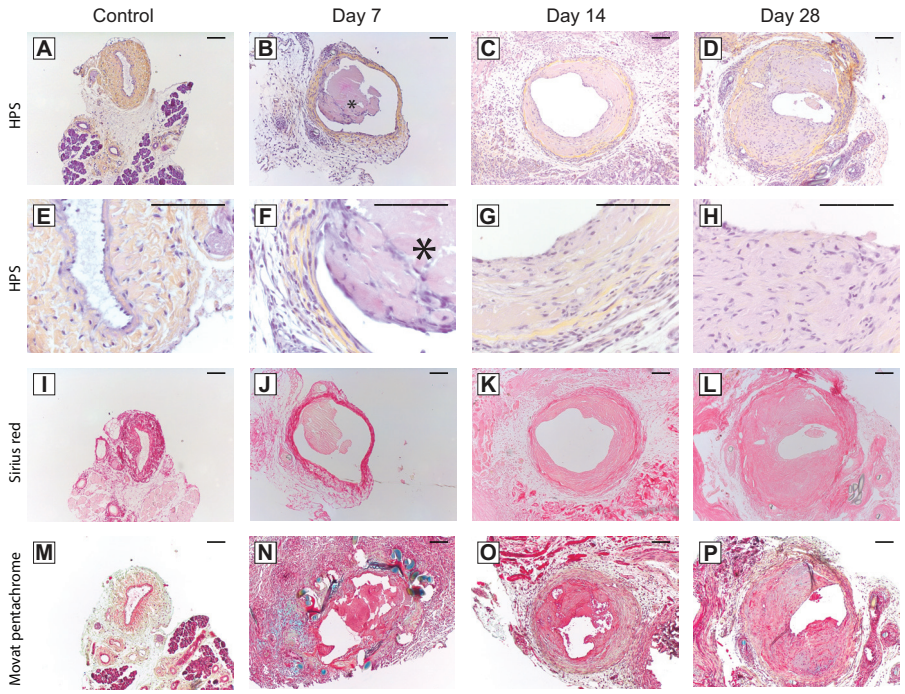

Figure 5. Outward remodeling (OR), intimal hyperplasia (IH), and collagen distribution are shown in time. Venous sections stained with hematoxylin, phloxine, and saffron (HPS) at days 7, 14 and 28 after creation of arteriovenous fistula (AVF). A control vein (A) before arterialization shows no IH and has a modest circumference compared with the veins (B-D) after AVF placement. OR was primarily observed at (B) day 7 and (C) day 14 and was less evident at (D) day 28. E-H, Higher magnification photomicrographs of panels (A-D) shows the development of neo-IH, which starts with a (F) thrombus that has been repopularized with cells as time progresses. I-L, Sirius red staining shows the collagen content in time. M-P, Movat pentachrome staining shows fibrin-rich areas (*bright red*) in the intimal lesion at the different time points. (A-D, I-P: original magnification, ×100; E-H: original magnification, ×400). Partially repopularized thrombus indicated by *asterisk* (*), and *black arrow* indicates fibrin-rich area. *Scale bar*: 100 μm.

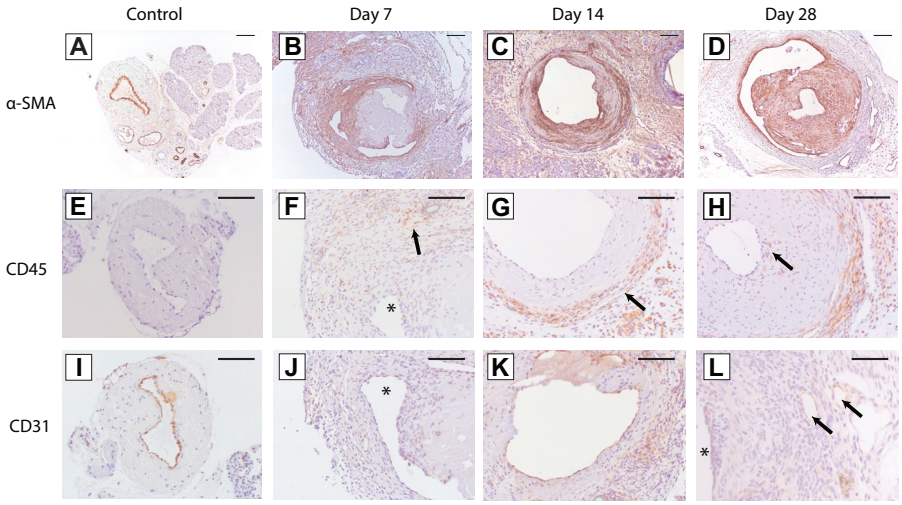

Figure 6. Immunohistochemical stainings. (A), Immunohistochemical assessment of cells positive for α-smooth muscle actin (*SMA*) revealed a small band in the control vein, compared with a (B-D) time-dependant increase of α-SMA-positive cells in the intimal hyperplasia (IH) after arteriovenous fistula (AVF) surgery. (E), The presence of leukocytes, which was absent in the control vein, was located in the (F-H) media and adventitia of the AVF vein at all time points. (H), However, leukocytes were also found in the intima at day 14 and 28 as depicted by the *black arrow*. (J) and (K), The luminal lining with cluster of differentiation (*CD*)31-positive endothelial cells, was disrupted at all time points but showed re-endothelialization in a time dependant manner. (L), Adventitial capillaries were present at all time points (*black arrow*). (I), The control vein showed an intact lining of endothelial cells. (A-D: original magnification, ×100; E-L: original magnification, ×200). The *asterisk* (*) indicates the lumen. *Scale bar*: 100 μm.

Composition of intimal hyperplasia

Histological analysis revealed a dynamic composition of the intimal lesions. Starting from day 7 the intimal lesion consisted mainly of an acellular fibrin-rich layer, consistent with a focal adherent thrombus (Fig 5, *B,F,N-P*). Concomitant with increased lesion size at later time points (day 14 and 28), progressive cellular density was observed (Fig 5, *F-H*). The majority of cells within the intima were α-sma-positive (Fig 6, *B-D*). Analysis of CD45-stained sections demonstrated the presence of leukocytes, mainly in the adventitia and outer circumference of the vessel wall at all time points and in the intima starting at day 14 (Fig 6, *F-H*). The endothelial layer was disrupted at all time points, although CD31(+) cells did increase in time. Furthermore, starting from day 7, an increased density of adventitial capillaries was observed (Fig 6, *J-L*).

Quantification of collagen content in the venous outflow tract revealed a time-dependent increase in absolute collagen content (Fig 3, *J-K* and Fig 5, *J-L*). However, no differences in collagen-positive area were observed between the control group and all time points were expressed as a percentage of the total vessel area. Thus, the relative contribution of collagen in the total vessel composition remained stable.

Discussion

In the present study, we describe a novel murine model of AVF failure in which the AVF configuration resembles the human situation (venous end to arterial side). We observed that the venous outflow tract of AVFs is characterized by OR in the first 14 days. Furthermore, we hypothesize that focal adherent thrombi appear to serve as fertile soil for the formation of progressive α-sma positive intimal lesions ultimately leading to a 50% loss of patency at 28 days after surgery.

Anticoagulant therapy was necessary for creating a patent AVF and finding the correct balance between acute thrombosis and hemorrhage proved to be of crucial importance. Importantly, we observed a very high incidence 69% of bleeding complications when using acetylsalicylic acid. Therefore, as an alternative, we administered a single dose of heparin which was effective in preventing acute thrombosis. Using our protocol with heparin, we observed early thrombosis and bleeding complications in 3% and 7% of the mice, respectively.

Outward remodeling

Although IH is widely considered to be the most important determinant of AVF failure, the functionality of the AVF is generally determined by the luminal area, which is defined by the net result of OR and IH formation. To the best of our knowledge, we are the first to quantify OR by measuring the circumference of the venous outflow tract in murine AVF. Studies in rats and mice have revealed that OR is induced by the increase in flow that evokes an adaptive response of the vessel in which the luminal diameter increases in attempt to reduce wall shear stress to pre-AVF levels [8, 25, 26]. In our study, we observed a 1.4-fold increase in venous circumference within 7 days after AVF placement. Unfortunately, data on wall shear stress could not be collected in this study. The decrease in OR at later time points could be the result of the partial normalization of shear stress levels as previously observed in murine [26] and human [27] AVF studies. Furthermore, we observed fragmentation of the IEL of the venous outflow tract, a phenomenon that has been described in previous studies [28-30]. This effect is likely driven by flow-induced matrix metalloproteinase (MMP)-2 and MMP-9 activation, a process that is

essential in facilitating outward remodeling [28, 29]. In keeping with this notion, serum levels of MMP-2 have been shown to be significantly higher in patients with matured AVFs as compared to non-matured AVFs [31].

We observed a smaller venous circumference in the occluded AVFs at 4 weeks after surgery. The latter might suggests that the cause of AVF failure in these cases could potentially be the result of impaired OR. However, these data should be interpreted with caution since we cannot exclude the possibility that the circumference decreased upon occlusion of the vessel.

Intimal hyperplasia formation

In failing human AVFs, IH is designated as one of the main contributors in the pathophysiology and is typically located in the juxta-anastomotic area of the venous outflow tract [32, 33]. In our study, progressive IH developed in this same region of the AVF, illustrating the resemblance to failing human fistulas.

Interestingly, we observed a remarkable pattern in the development of IH not previously described in AVF studies. In our murine AVFs, IH appears to commence with the focal adherence of thrombi. In the following weeks, these lesions showed progressive cellularity, culminating in a high cellular density at 28 days after surgery. At this time, intimal lesions possessed the hallmarks of classic IH of failed human AVFs, as evidenced by the presence of high numbers of α-sma(+) cells [32, 34].

Thus far, IH is considered primarily to be the direct result of migrating and proliferating VSMCs, and that thrombus formation in the early phase after surgery would be considered a separate entity [5, 11, 13, 35]. Although the venous morphology in the early phase after AVF surgery has not been described in great detail in humans, the sequence of events in the development of IH in our study does resemble the pathophysiology of intimal lesions after (arterial) angioplasty and in vein grafts [36, 37]. Furthermore, Castier et al. also showed partly acellular lesions in the venous outflow tract of murine AVF [5]. The adherence of small (platelet and fibrin-rich) thrombi to the vessel wall most likely results from endothelial denudation and the subsequent exposure of the subendothelial matrix leading to platelet adhesion and activation [36, 38, 39]. Indeed, we observed marked endothelial denudation in the venous outflow tract in the first 7 days after surgery, a phenomenon that also was observed in previous animal studies of AVF failure [8, 11].

This observation might suggests that anticoagulatory interventions could be an eligible strategy to inhibit intimal hyperplasia. Previous studies in a murine vascular endothelial injury model indeed revealed reduced IH upon treatment with human soluble CD39, an inhibitor of ADP-mediated platelet activation [40]. In contrast, a randomized clinical controlled trial by Dember et al. showed no significant effect on AVF maturation, despite a reduction in incidence of early thrombosis in patients treated with clopidogrel [41]. In our opinion, the limited effect of

systemic antiplatelet therapy on AVF maturation in humans does not necessarily preclude a contributing role of platelets in local development of IH in AVF.

Role of inflammation in vascular adaptation in arteriovenous fistulas

The inflammatory response is a crucial process involved in vascular injury and is linked to development of IH [37, 39, 42]. Upon injury, leukocytes are recruited via activated platelets lining the denudated endothelium and release chemokines such as MCP-1 [43], IL-6 and IL-8, which further stimulates leukocyte recruitment [42]. Similar to the pathophysiology in occlusive vein graft disease and arterial restenosis, we observed a marked influx of leukocytes at the adventitial side of the vein throughout all time points. In contrast, hardly any CD45(+) cells were present in the intima in the first 14 days. This might suggests that leukocyte infiltration in the early phase predominantly occurs via adventitial capillaries rather than the lumen [44, 45] such as demonstrated by Gotoh et al. [45]. However, the role of inflammation in outward remodeling in the AVF has gained little attention. Future experiments using anti-inflammatory therapeutic agents could aid in the elucidation of the contribution of inflammation in AVF remodeling.

Animal models

In concordance with other rodent AVF models [5, 7, 8, 11-13], we observed rapid development of IH. Furthermore, as previously described in AVF studies in rats 8, marked venous OR was observed in the first 14 days following surgery. As a result of this venous OR, we observed an increase in luminal area in the first 14 days, whereas Castier et al. described a decrease in luminal area from the first week after AVF creation[5]. In Castier's study however, the arterial rather than the venous segment of the AVF was analyzed. Together with the difference in AVF configuration, this might explain the observed difference in luminal area since previous studies in rats have revealed that arterial OR is less prominent than venous OR. [8] However, this explanation remains speculative since no data on OR were reported by Castier et al.

Near infrared fluorescence imaging

We were unable to visualize the AVF with conventional techniques such as ultrasonography (US) and magnetic resonance imaging (MRI). Therefore, we utilized NIRF technology, which proved to be a quick and accurate method to assess the patency of murine AVFs.

Study limitation

Although animal models are useful in gaining insight into the pathophysiology of various human diseases, we should remain cautious in the interpretation and extrapolation, as the pathology in animals does not necessarily mimic to that of humans.

A multitude of risk factors, including the uremic milieu and the hemodialysis procedure itself are likely to contribute to premature vascular diseases [46, 47]. Uremia can play a major role in this regard, and more specifically can directly lead to venous IH in end stage renal disease patients prior to hemodialysis access surgery [48]. For future studies, incorporation of chronic renal failure in mice as described by Kokubo et al. [35] will be considered.

The complex microsurgical procedure remains a challengeable one that requires a skilled surgeon. However, the surgical difficulty is comparable to the existing murine AVF model as described by Castier [5]. Importantly, sufficient training has led to a surgical success rate during ongoing experimental studies of 97%.

In conclusion, we describe a novel murine AVF model with a similar configuration as is used most frequently in humans. This end-to-side configuration, while providing a more accurate reflection of human AVF pathophysiology, can also yield novel insight into this process by being effectively applied in a myriad of transgenic animals. In view of the different proposed mechanisms that are involved in venous remodeling in the AVF, disabling genes that play an important role in coagulation, inflammation and VSMC biology can help us to elucidate the complex pathophysiology of AVF failure. The obtained knowledge from these studies will hopefully result in the development of new therapeutic strategies that improve the patency of AVFs in patients that require hemodialysis.

Acknowledgments

This study was supported by a grant from the Dutch Kidney Foundation (KJPB 08.0003).

We thank Carolien Rothuizen for her contribution to the study; Hoang Pham for his assistance with the pathology work-up; and Eric van der Veer for his valuable review of the manuscript.

Reference List

1. Asif A, Roy-Chaudhury P, Beathard GA. Early arteriovenous fistula failure: a logical proposal for when and how to intervene. *Clin J Am Soc Nephrol* 2006;1:332-9.

2. Falk A. Maintenance and salvage of arteriovenous fistulas. *J Vasc Interv Radiol* 2006;17:807-13.

3. Tordoir JH, Rooyens P, Dammers R, van der Sande FM, de HM, Yo TI. Prospective evaluation of failure modes in autogenous radiocephalic wrist access for haemodialysis. *Nephrol Dial Transplant* 2003;18:378-83.

4. Dixon BS, Novak L, Fangman J. Hemodialysis vascular access survival: upper-arm native arteriovenous fistula. *Am J Kidney Dis* 2002;39:92-101.

5. Castier Y, Lehoux S, Hu Y, Foteinos G, Tedgui A, Xu Q. Characterization of neointima lesions associated with arteriovenous fistulas in a mouse model. *Kidney Int* 2006;70:315-20.

6. Johnson MS, McLennan G, Lalka SG, Whitfield RM, Dreesen RG. The porcine hemodialysis access model. *J Vasc Interv Radiol* 2001;12:969-77.

7. Kwei S, Stavrakis G, Takahas M, Taylor G, Folkman MJ, Gimbrone MA, Jr., et al. Early adaptive responses of the vascular wall during venous arterialization in mice. *Am J Pathol* 2004;164:81-9.

8. Langer S, Heiss C, Paulus N, Bektas N, Mommertz G, Rowinska Z, et al. Functional and structural response of arterialized femoral veins in a rodent AV fistula model. *Nephrol Dial Transplant* 2009;24:2201-6.

9. Lemson MS, Daemen MJ, Kitslaar PJ, Tordoir JH. A new animal model to study intimal hyperplasia in arteriovenous fistulas. *J Surg Res* 1999;85:51-8.

10. Lin T, Horsfield C, Robson MG. Arteriovenous fistula in the rat tail: a new model of hemodialysis access dysfunction. *Kidney Int* 2008;74:528-31.

11. Manning E, Skartsis N, Orta AM, Velazquez OC, Liu ZJ, Asif A, et al. A new arteriovenous fistula model to study the development of neointimal hyperplasia. *J Vasc Res* 2012;49:123-31.

12. Misra S, Fu AA, Anderson JL, Sethi S, Glockner JF, McKusick MA, et al. The rat femoral arteriovenous fistula model: increased expression of matrix metalloproteinase-2 and -9 at the venous stenosis. *J Vasc Interv Radiol* 2008;19:587-94.

13. Nath KA, Kanakiriya SK, Grande JP, Croatt AJ, Katusic ZS. Increased venous proinflammatory gene expression and intimal hyperplasia in an aorto-caval fistula model in the rat. *Am J Pathol* 2003;162:2079-90.

14. Ramacciotti E, Galego SJ, Gomes M, Goldenberg S, De Oliveira GP, Pinto OJ. Fistula size and hemodynamics: an experimental model in canine femoral arteriovenous fistulas. *J Vasc Access* 2007;8:33-43.

15. Tronc F, Wassef M, Esposito B, Henrion D, Glagov S, Tedgui A. Role of NO in flow-induced remodeling of the rabbit common carotid artery. *Arterioscler Thromb Vasc Biol* 1996;16:1256-62.

16. Wang Y, Krishnamoorthy M, Banerjee R, Zhang J, Rudich S, Holland C, et al. Venous stenosis in a pig arteriovenous fistula model--anatomy, mechanisms and cellular phenotypes. *Nephrol Dial Transplant* 2008;23:525-33.

17. Yang B, Shergill U, Fu AA, Knudsen B, Misra S. The mouse arteriovenous fistula model. *J Vasc Interv Radiol* 2009;20:946-50.

18. Kang L, Yamada S, Hernandez MC, Croatt AJ, Grande JP, Juncos JP, et al. Regional and systemic hemodynamic responses following the creation of a murine arteriovenous fistula. *Am J Physiol Renal Physiol* 2011;301:F845-F851.

19. Krishnamoorthy MK, Banerjee RK, Wang Y, Zhang J, Roy AS, Khoury SF, et al. Hemodynamic wall shear stress profiles influence the magnitude and pattern of stenosis in a pig AV fistula. *Kidney Int* 2008;74:1410-9.

20. Sivanesan S, How TV, Bakran A. Sites of stenosis in AV fistulae for haemodialysis access. *Nephrol Dial Transplant* 1999;14:118-20.

21. Ene-Iordache B, Cattaneo L, Dubini G, Remuzzi A. Effect of anastomosis angle on the localization of disturbed flow in 'side-to-end' fistulae for haemodialysis access. *Nephrol Dial Transplant* 2012.

22. Ene-Iordache B, Remuzzi A. Disturbed flow in radial-cephalic arteriovenous fistulae for haemodialysis: low and oscillating shear stress locates the sites of stenosis. *Nephrol Dial Transplant* 2012;27:358-68.

23. Gioux S, Kianzad V, Ciocan R, Gupta S, Oketokoun R, Frangioni JV. High-power, computer-controlled, light-emitting diode-based light sources for fluorescence imaging and image-guided surgery. *Mol Imaging* 2009;8:156-65.

24. Troyan SL, Kianzad V, Gibbs-Strauss SL, Gioux S, Matsui A, Oketokoun R, et al. The FLARE intraoperative near-infrared fluorescence imaging system: a first-in-human clinical trial in breast cancer sentinel lymph node mapping. *Ann Surg Oncol* 2009;16:2943-52.

25. Guzman RJ, Abe K, Zarins CK. Flow-induced arterial enlargement is inhibited by suppression of nitric oxide synthase activity in vivo. *Surgery* 1997;122:273-9.

26. Castier Y, Brandes RP, Leseche G, Tedgui A, Lehoux S. p47phox-dependent NADPH oxidase regulates flow-induced vascular remodeling. *Circ Res* 2005;97:533-40.

27. Corpataux JM, Haesler E, Silacci P, Ris HB, Hayoz D. Low-pressure environment and remodelling of the forearm vein in Brescia-Cimino haemodialysis access. *Nephrol Dial Transplant* 2002;17:1057-62.

28. Tronc F, Mallat Z, Lehoux S, Wassef M, Esposito B, Tedgui A. Role of matrix metalloproteinases in blood flow-induced arterial enlargement: interaction with NO. *Arterioscler Thromb Vasc Biol* 2000;20:E120-E126.

29. Martin BJ, Stehbens WE, Davis PF, Ryan PA. Scanning electron microscopic study of hemodynamically induced tears in the internal elastic lamina of rabbit arteries. *Pathology* 1989;21:207-12.

30. Rotmans JI, Velema E, Verhagen HJ, Blankensteijn JD, de Kleijn DP, Stroes ES, et al. Matrix metalloproteinase inhibition reduces intimal hyperplasia in a porcine arteriovenous-graft model. *J Vasc Surg* 2004;39:432-9.

31. Lee ES, Shen Q, Pitts RL, Guo M, Wu MH, Sun SC, et al. Serum metalloproteinases MMP-2, MMP-9, and metalloproteinase tissue inhibitors in patients are associated with arteriovenous fistula maturation. *J Vasc Surg* 2011;54:454-9.

32. Roy-Chaudhury P, Arend L, Zhang J, Krishnamoorthy M, Wang Y, Banerjee R, et al. Neointimal hyperplasia in early arteriovenous fistula failure. *Am J Kidney Dis* 2007;50:782-90.

33. Beathard GA, Arnold P, Jackson J, Litchfield T. Aggressive treatment of early fistula failure. *Kidney Int* 2003;64:1487-94.

34. Roy-Chaudhury P, Wang Y, Krishnamoorthy M, Zhang J, Banerjee R, Munda R, et al. Cellular phenotypes in human stenotic lesions from haemodialysis vascular access. *Nephrol Dial Transplant* 2009;24:2786-91.

35. Kokubo T, Ishikawa N, Uchida H, Chasnoff SE, Xie X, Mathew S, et al. CKD accelerates development of neointimal hyperplasia in arteriovenous fistulas. *J Am Soc Nephrol* 2009;20:1236-45.

36. Mitra AK, Gangahar DM, Agrawal DK. Cellular, molecular and immunological mechanisms in the pathophysiology of vein graft intimal hyperplasia. *Immunol Cell Biol* 2006;84:115-24.

37. Muto A, Model L, Ziegler K, Eghbalieh SD, Dardik A. Mechanisms of vein graft adaptation to the arterial circulation: insights into the neointimal algorithm and management strategies. *Circ J* 2010;74:1501-12.

38. Wilentz JR, Sanborn TA, Haudenschild CC, Valeri CR, Ryan TJ, Faxon DP. Platelet accumulation in experimental angioplasty: time course and relation to vascular injury. *Circulation* 1987;75:636-42.

39. Patel SD, Waltham M, Wadoodi A, Burnand KG, Smith A. The role of endothelial cells and their progenitors in intimal hyperplasia. *Ther Adv Cardiovasc Dis* 2010;4:129-41.

40. Drosopoulos JH, Kraemer R, Shen H, Upmacis RK, Marcus AJ, Musi E. Human solCD39 inhibits injury-induced development of neointimal hyperplasia. *Thromb Haemost* 2010;103:426-34.

41. Dember LM, Beck GJ, Allon M, Delmez JA, Dixon BS, Greenberg A, et al. Effect of clopidogrel on early failure of arteriovenous fistulas for hemodialysis: a randomized controlled trial. *JAMA* 2008;299:2164-71.

42. Welt FG, Rogers C. Inflammation and restenosis in the stent era. *Arterioscler Thromb Vasc Biol* 2002;22:1769-76.

43. Juncos JP, Grande JP, Kang L, Ackerman AW, Croatt AJ, Katusic ZS, et al. MCP-1 contributes to arteriovenous fistula failure. *J Am Soc Nephrol* 2011;22:43-8.

44. Maiellaro K, Taylor WR. The role of the adventitia in vascular inflammation. *Cardiovasc Res* 2007;75:640-8.

45. Gotoh R, Suzuki J, Kosuge H, Kakuta T, Sakamoto S, Yoshida M, et al. E-selectin blockade decreases adventitial inflammation and attenuates intimal hyperplasia in rat carotid arteries after balloon injury. *Arterioscler Thromb Vasc Biol* 2004;24:2063-8.

46. Kennedy R, Case C, Fathi R, Johnson D, Isbel N, Marwick TH. Does renal failure cause an atherosclerotic milieu in patients with end-stage renal disease? *Am J Med* 2001;110:198-204.

47. Cheung AK, Sarnak MJ, Yan G, Dwyer JT, Heyka RJ, Rocco MV, et al. Atherosclerotic cardiovascular disease risks in chronic hemodialysis patients. *Kidney Int* 2000;58:353-62.

48. Lee T, Chauhan V, Krishnamoorthy M, Wang Y, Arend L, Mistry MJ, et al. Severe venous neointimal hyperplasia prior to dialysis access surgery. *Nephrol Dial Transplant* 2011;26:2264-70.

Supplemental Data

Surgical procedure

After anesthetizing the mice, we covered the eyes with a sterile ointment and shaved the surgical area. Next, the animal was fixed in a supine position on a heating blanket. The skin was then disinfected with ethanol and a ventral midline incision was made in the neck under a dissecting microscope (M80, Leica, Wetzlar, Germany). After dissecting the dorsomedial distal branch of the right external jugular vein, a vascular clamp (B1-V, S&T, Neuhausen, Switzerland) was placed proximally and a 10.0 ligature (BBraun, Melsungen, Germany) was placed distally followed by transection of the vein just proximal from the ligature. (Fig 1, A-E) The vein was then rinsed with saline containing 100 IU/ml heparin.

The right sternocleidomastoid muscle was then resected with a cauterizer (Fine Science Tools, Heidelberg, Germany). Next, the right common carotid artery was dissected and clamped, followed by an incision with a micro-scissor (Fine Science Tools, Heidelberg, Germany) of approximately 1.0 mm longitudinally. Subsequently, the carotid artery was rinsed with saline containing 100 IU/ml heparin, whereupon the end of the vein was anastomized to the side of the artery using 10.0 interrupted sutures. The first two interrupted sutures were inserted at the twelve- and six o'clock position of the vein and at the ends of the incision in the artery, providing mild tissue tension and a good starting position by dividing the suture area of the vein in two even portions. Tension was then also applied longitudinally using a 6.0 suture thread (BBraun, Melsungen, Germany) that was placed below the vein, and was followed by placing interrupted 10.0 sutures at the exposed half of the anastomosis. Next, heparin was injected intravenously in the femoral vein at a dose of 0.2 IU/gram bodyweight. The rear unexposed part of the anastomosis was then exposed by a 180 degrees axial rotation of the arterial clamps and the partly anastomosed vein with the help of a suture thread that now is placed above the vein and below the artery. The venous clamp was removed during the rotational procedure. After completion of the anastomosis, the remaining arterial clamps were removed starting with the distal clamp. After confirming the patency of the AVF, the skin was closed with a 6.0 running suture (BBraun, Melsungen, Germany).

Immunohistochemistry

For immunohistochemical stainings, deparaffinization and hydration was followed by a treatment with 1% hydrogen peroxide and 5% bovine serum albumine in order to block the endogenous peroxidase and aspecific binding sites respectively. Antigen retrieval in the anti-CD31 and CD45 staining consisted of a treatment with 0.1% trypsin (Sigma-Aldrich, St. Louis, MO, USA) for 30 minutes at 37 degrees Celsius.

Incubation of the primary antibodies was performed overnight at room temperature. Subsequently, sections were incubated at room temperature for 1 hour with HRP labeled antibodies against: mouse IgG (Dako, Glostrup, Denmark) in the α-smooth muscle actin staining at 1:1000 dilution and rabbit IgG (Envision, Dako, Glostrup, Denmark) in the staining against CD31 Biotinylated anti rat antibody (Vector laboratories, Burlingame, CA, USA) was used in the stainings against CD45, followed by a treatment with a 0.2 % streptavidin-AB complex (Dako, Glostrup, Denmark) for 30 minutes at room temperature. Immunoreactive tissue was then developed by using a DAB peroxidase substrate kit (Dako, Glostrup, Denmark). Sections were counterstained with hematoxylin.

Near infrared fluoroscopy

Video 1

Visualization of a patent arteriovenous fistula directly after creation using near infrared fluorescence imaging. Two hundred μL of indocyanine green adsorbed to human serum albumin (500μM) was injected intravenously in the femoral vein. The fluorescent signal signal of indocyanine green was pseudo-colored green and merged with the color video.

Video 2

Visualization of a patent arteriovenous fistula 28 days after creation using near infrared fluorescence imaging. Two hundred μL of indocyanine green adsorbed to human serum albumin (500μM) was injected intravenously in the femoral vein seconds after the start of the recording. The fluorescent signal signal of indocyanine green was pseudo-colored green and merged with the color video. The video shows direct antegrade filling of the venous outflow tract demonstrating a patent arteriovenous fistula.